

Antibacterial and Bioactive Coatings Based on Radio Frequency Co-Sputtering of Silver Nanocluster-Silica Coatings on PEEK/Bioactive Glass Layers Obtained by Electrophoretic Deposition

Muhammad Atiq Ur Rehman,[†] Sara Ferraris,[‡] Wolfgang H. Goldmann,[§] Sergio Perero,[‡] Fatih Erdem Bastan,^{†,||} Qaisar Nawaz,[†] G. Gautier di Confienzo,[⊥] Monica Ferraris,[‡] and Aldo R. Boccaccini^{*,†,||}

[†]Institute of Biomaterials, Department of Material Science and Engineering, University of Erlangen-Nuremberg, Cauerstrasse 6, 91058 Erlangen, Germany

[‡]Institute of Materials Physics and Engineering, Department of Applied Science and Technology, Politecnico di Torino, 10129 Torino, Italy

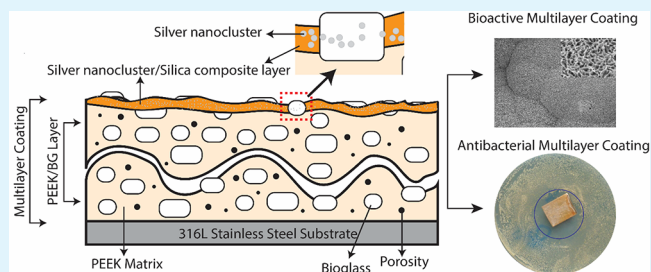
[§]Department of Biophysics, University of Erlangen-Nuremberg, Henkstrasse 91, 91052 Erlangen, Germany

^{||}Engineering Faculty, Department of Metallurgy and Materials Engineering, Thermal Spray Research and Development Laboratory, Sakarya University, 54187 Esentepe, Sakarya, Turkey

[⊥]CNR, IMAMOTER, Turin 10135, Italy

ABSTRACT: Bioactive and antibacterial coatings on stainless steel substrates were developed and characterized in this study. Silver nanocluster–silica composite coatings of 60–150 nm thickness were deposited using radio frequency (RF) co-sputtering on PEEK/bioactive glass (BG) layers (of 80–90 μm thickness) which had been electrophoretically deposited onto stainless steel. Two sputtering conditions were used by varying the deposition time (15 and 40 min); the resulting microstructure, composition, adhesion strength, in vitro bioactivity, and antibacterial activity were investigated. Scanning electron microscopy (SEM), X-ray photoelectron spectroscopy (XPS), and energy dispersive spectroscopy (EDX) confirmed the presence of silver nanoclusters, which were homogeneously embedded in the silica matrix. The isoelectric point of the coatings and their charge at physiological pH were determined by zeta potential measurements. The presence of BG particles in the PEEK/BG layer allows the coatings to form apatite-like crystals upon immersion in simulated body fluid (SBF). Moreover, silver nanoclusters embedded in the silica matrix as a top layer provided an antibacterial effect against *Escherichia coli* and *Staphylococcus carnosus*.

KEYWORDS: antibacterial coatings, bioactive coatings, RF sputtering, silver, PEEK, bioactive glass, electrophoretic deposition



1. INTRODUCTION

In orthopedic implants, most infections occur due to the growth of bacterial biofilms, which may lead to the failure of the implant. It is imperative to resist the growth of biofilms because of their resistance to the immune system and antibiotics.^{1–5} Systemic drug administration is not always effective due to impaired blood circulation at the site of injury and a relatively low concentration of drug at the desired site. Local delivery of drugs, metallic ions, and biomolecules is considered an effective approach to treat infections because local delivery systems maintain the high concentration of bioactive agent at the desired site. Moreover, local drug delivery offers controlled release of drugs, which reduces the risk of toxicity.^{1,6} A widely investigated approach to avoid infections at the site of injury involves impregnating the implant with antibiotics prior to implantation.² This approach is certainly useful, yet a key challenge exists to develop orthopedic implants that can exert a

long-term antibacterial effect in order to prevent late infections.^{1,7–9} Furthermore, the widespread use of antibiotics has led to the development of antibacterial resistant bacterial strains, which have recently been indicated as a “global threat”; therefore, there is a pressing need for investigating alternative strategies to treat bacterial infections.^{1,4,6,10}

Silver exhibits antibacterial activity at low concentrations against a broad spectrum of Gram-positive and Gram-negative bacteria without being toxic to cells.^{1–3,11} Silver ions can bind to thiol groups, which cause the death of bacteria; i.e., Ag^+ (silver ion) can bind to proteins, altering their structure, causing rupture of bacteria walls, and eventually preventing the function of DNA associated with bacteria division and

Received: June 15, 2017

Accepted: August 31, 2017

Published: August 31, 2017

replication.^{1,12–14} Silver can be applied as salts and in complexes, but silver in nanoparticulate form has gained increasing attention in recent years.^{1,15,16} The antibacterial properties of silver nanoparticles relate to the extremely high surface area to volume ratio, which can trigger the release of silver ions. Silver in its metallic form is inert, but quite often it is converted to an ionic form due to its interaction with moisture. Moreover, silver ions are highly reactive and attach to the surface or enter into the bacteria causing membrane rupture and damage.^{3,15,17} The antibacterial activity of silver nanoparticles depends on both the dimensions and shape.^{1,18} Despite a widespread use of nanosilver based products in numerous applications, limited information about their potential toxicity is available, and safety concerns should be considered.^{19,20} Therefore, controlled release of silver ions must be addressed prior to its successful use in orthopedic applications.

Radio frequency (RF) co-sputtering is one of the most versatile coating methods for achieving thin films of nanocomposites at low temperatures, which is particularly useful for polymeric substrates.^{3,21–23} In this process, first, a vacuum is created in the chamber with the help of argon gas followed by the application of a very high electric field, which ionizes the argon gas and creates plasma inside the chamber. Ions of argon strike the target at relatively high velocity thus extracting the atoms, which are subsequently deposited on the substrate. Deposition parameters, such as plasma power, atmosphere, pressure, etc., can be controlled easily to tailor the thin film morphology and properties.^{2,3,12,16,24,25}

In previous studies some of the authors developed silver nanocluster-silica composite coatings by means of a radio frequency (RF) co-sputtering technique.^{2,3} The silver nanoclusters were well-embedded into the silica matrix, which provides good mechanical properties, thermal resistance, and controlled release of silver ions, without the release of potentially toxic silver nanoparticles. Furthermore, this technique can be applied to almost all kinds of substrates, and the silver contents in the coatings can be controlled by process parameters (e.g., deposition time).^{6,16,21,25,26} Recently, a three-layer system of nanocrystalline hydroxyapatite, silver nanoparticles, and calcium phosphate was deposited on titanium by the combination of electrophoretic deposition (EPD) and RF magnetron sputtering.²⁷

EPD is a useful technique to form biocompatible and bioactive composite coatings on complex shaped and porous substrates under ambient conditions.^{5,8,9,28–30} In EPD, charged particles in stable suspension (high value of zeta potential) move toward the oppositely charged electrode under the influence of an applied electric field.^{5,31} Polyetheretherketone (PEEK) and bioactive glass (BG) composite coating were first developed by Boccaccini et al. utilizing EPD.³² Recently, we have investigated the kinetics of the EPD process and co-deposition mechanism of PEEK and BG particles by applying a novel Taguchi design of experiment (DoE) approach.³³

The focus of the present research work is to obtain antibacterial coatings on PEEK/BG composite layers (deposited by EPD on 316L SS) by using an RF co-sputtering technique to develop nanoscale silver nanoclusters/silica composite coatings on PEEK/BG layers. The bottom layer contains 25 wt % PEEK and 75 wt % BG particles. The top layer contains silver particles embedded in the silica matrix with a Ag/(Ag + Si) atomic ratio of 0.037 ± 0.015 . The Ag/(Ag + Si) atomic ratio was deduced from the literature for the

sputtering conditions applied in this study, because the sputtering process is not affected by the change in substrate materials.²⁵ Preliminary in vitro bioactivity and antibacterial studies yielded promising results to be further considered for clinical applications. To the best of the authors' knowledge, a combination of EPD and RF sputtering has never been used before to attain multifunctional bioactive and antibacterial coatings; thus, the coating technology presented in this study is novel. This novel combination of PEEK/BG coatings with silver nanocluster-silica composite coatings should (i) reduce the stress shielding effect, (ii) improve the biostability, and (iii) enhance the in vitro bioactivity of the surface due to the PEEK/BG layer.³³ Moreover, the top layer (silver nanocluster-silica composite) will provide the controlled release of silver ions due to the fact that silver particles are embedded in the silica matrix, which will reduce potential cytotoxic effects.⁶ EPD was selected for depositing thick (80–90 μm) PEEK/BG layers on stainless steel, because it allows the codeposition of polymer particles along with inorganic particles in a relatively short time period under ambient conditions. The RF sputtering was utilized to coat nanoscale silver-silica composite coatings because it allows coating uniform films on almost all kind of substrate materials.

2. EXPERIMENTAL PROCEDURE

2.1. EPD of PEEK/BG. A portion of 2 wt % PEEK powder (mean particle size of 10 μm , 704XF Victrex) and 6.67 wt % bioactive glass 45S5 powder (2 μm average particle size, Schott, Germany) with nominal composition of $45 \text{ SiO}_2\text{--}24.5 \text{ Na}_2\text{O--}24.5 \text{ CaO--}6 \text{ P}_2\text{O}_5$ (wt %) were mixed in ethanol. A portion of 13.32 wt % citric acid powder (monohydrate, VWR International) was added in ethanol to form a stable suspension for EPD. The addition of citric acid leads to negative charging of PEEK and BG particles. The stability of suspensions was determined by zeta-potential measurements using a zetasizer (nano ZS equipment, Malvern Instruments, UK). Stainless steel (SS) foils (316L) were used as substrates and counter electrodes (deposition area 175 mm^2) for constant voltage EPD. An interelectrode spacing of 0.5 cm, deposition voltage of 110 V, and deposition time of 120 s (following the previous studies) in the EPD experiments^{4,33,35,36} were used. The coatings were sintered in a furnace (Nabertherm GmbH) at 400 $^\circ\text{C}$ for 30 min with a ramp rate of 2 $^\circ\text{C}/\text{min}$, in air (the details about the optimization of sintering temperature are not shown here).

2.2. RF Co-Sputtering of Silver Nanoclusters-Silica Composite. Radio frequency (RF) co-sputtering (Microcoat MS450) was the method of choice to deposit silver nanocluster-silica composite on PEEK/BG layer (PEEK/BG/Ag). Silver (Sigma-Aldrich 99.99%) and silica (Franco Corradi s.r.l. 99.99%) targets were used to deposit silver nanocluster-silica composite coatings. First, very low pressure was developed (10^{-5} Pa) in the deposition chamber, and then pure argon gas was introduced, which maintains a dynamic pressure at $10^{-2}/10^{-1}$ Pa. Second, an electric field was applied in the chamber in order to obtain plasma, from which Ar^+ ions were produced. These ions were accelerated by an applied electric field and collided with the surface of the target, which led to an atom or a cluster of atoms being extracted. Finally, the extracted material was deposited on the substrate and formed a thin composite film. In the case of a nonconductive target (e.g., silica), radio frequency (RF) sputtering was used. The applied RF power on silica target was 200 W, but for depositing silver dc power of 1 W was used at the silver target. To avoid the excess of silver deposition, the plasma over silver target was switched on for 1 s after every 24 s during the whole deposition time. The low chemical affinity between silica and silver led to the production of silver nanoclusters embedded in the silica matrix. The deposition time was varied from 15 min (labeled PEEK/BG/Ag1) to 40 min (labeled PEEK/BG/Ag 2), which may yield a coating thickness of 60–150 nm.^{21,25} The two sputtering conditions (PEEK/BG/Ag1 and PEEK/BG/Ag2) were selected on the basis of previous results,^{22,25} because they were

antibacterial without being cytotoxic. In order to obtain two types of composites, namely, PEEK/BG/Ag1 and PEEK/BG/Ag2, the sputtering time was varied, while all other parameters were kept constant. The PEEK/BG/Ag1 composite coatings were obtained at a sputtering time of 15 min, whereas the PEEK/BG/Ag2 coatings were obtained at a sputtering time of 40 min. The increase in sputtering time will lead to an increase in the thickness of the coatings and consequently the total silver content in the coatings will increase too.

2.3. Characterization of the Coatings. The surface topography of the coatings was analyzed by field emission scanning electron microscope (FESEM, LEO 435VP, Carl Zeiss AG) at an energy of 10–15 kV. Samples were sputter-coated (Q150/S, Quorum Technologies) with chromium and gold prior to scanning electron microscopy (SEM) to prevent the effect of charging on the samples. Compositional analysis was performed qualitatively by energy dispersive X-ray spectroscopy (EDX) at 15 kV (LEO 435VP, Carl Zeiss AG) and Fourier transform infrared spectroscopy (FTIR) (Nicolet 6700, Thermo Scientific) in transmittance mode ranging from 4000 to 400 cm^{-1} . The crystallographic and surface analysis was performed by X-ray diffraction (XRD) investigations (D8 Advance, Bruker) in the range 20–80°. The chemical and compositional analysis was done by X-ray photoelectron spectroscopy (XPS, VSW TA10 nonmonochromatic Al $K\alpha$ (1486.6 eV) X-ray source).

Zeta potential versus pH measurements were performed for PEEK/BG and PEEK/BG/Ag1 and PEEK/BG/Ag2 with the streaming potential technique by means of an electrokinetic analyzer for solid samples (SurPASS, Anton Paar). A 0.001 M KCl solution was employed as the electrolyte, and diluted HCl (0.05 M) and NaOH (0.05 M) solutions were used for pH titration with the automatic instrument titration unit.

In order to evaluate the adhesion strength of the multilayer coatings scratch tests were performed in Revetest mode (CSM Revetest machine) on each sample. As far as scratch tests are concerned, a progressive load (1–50 N) was applied on the coated surface through a Rockwell C diamond indenter with 200 μm diameter. The total scratch length track was 5 mm, and the indenter speed was 5.2 mm/min. Three different tracks were performed on each sample (PEEK/BG/Ag1 and PEEK/BG/Ag2). Critical loads were determined through acoustic emission (AE) measurements and optical observations of the scratch.³ Two critical loads (L_{C1} and L_{C2}) were determined on each specimen: the first critical load (L_{C1}) corresponded to the load at which the first crack occurred while the second (L_{C2}) corresponded to the load at which the coating was completely removed from the scratch channel.

To access the acellular in vitro bioactivity of the coatings in terms of hydroxyapatite (HAP) formation, the samples were immersed in simulated body fluid (SBF), as proposed by Kokubo et al.³⁷ Coated samples (15 mm \times 15 mm \times 0.2 mm) were immersed in 50 mL of SBF and were then incubated at 37 °C for 1, 3, 7, and 14 days. At each time point samples were removed from SBF, rinsed with distilled water, and left to dry in air. The formation of an apatite-like layer was examined with SEM/EDX, XRD, and FTIR techniques after immersion in SBF. Finally, the effect of silver nanoclusters in the coatings was investigated by conducting the antibacterial test. The agar disk diffusion test was performed on PEEK/BG (control sample) and on PEEK/BG/Ag1 and PEEK/BG/Ag2 samples. Prior to this study, coatings were sterilized in PBS for 15 min and then rinsed with distilled water. Agar plates were filled with 20 mL of agar, and then 20 μL of LB-media (Gram-negative bacteria, *Escherichia coli*; Gram-positive, *Staphylococcus carnosus*) with optical density of 0.015 (OD_{600}) was spread homogeneously on the agar plate. Samples were placed on the prepared agar plate, and were kept in the incubator at 37 °C for 24 h. After 24 h of incubation, the zones of inhibition were measured by using “ImageJ” analysis (each test was performed in triplicate).

3. RESULTS AND DISCUSSION

3.1. PEEK/BG Composite Coatings on 316L SS. Figure 1A,B shows SEM images of PEEK/BG composite coatings at different magnifications. Figure 1B shows that sintered PEEK/

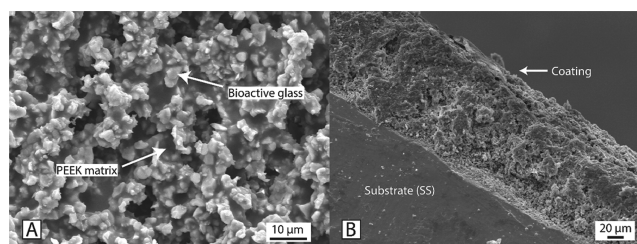


Figure 1. PEEK/BG composite coatings produced at an applied electric field of 220 V/cm for 120 s and sintered at 400 °C: (A) SEM image at surface and (B) SEM image at cross section.

BG coatings are homogeneous with a fairly homogeneous coating thickness. Moreover, coatings have high particle packing (Figure 1A) and uniform coating thickness of 80–90 μm (Figure 1B). The composition and thickness of the coatings were optimized by using the “design of experiment approach”, recently published.³³ The PEEK/BG layers were composed of 75 wt % BG and 25 wt % PEEK (the experimental details for determining the PEEK and BG content in the coatings were described in the previous study³³).

3.2. Silver Nanocluster-Silica Composite Coatings on PEEK/BG Layer by RF Co-Sputtering. RF co-sputtering was the method of choice for depositing thin antibacterial coatings on PEEK/BG layers. RF co-sputtering is considered a useful technique for depositing silver nanocluster-silica composite on different substrates.^{3,6,16,21,25} However, the uncontrolled release of silver ions may cause cell toxicity.^{1,4,22} The silver nanoclusters were embedded in the silica matrix to overcome the possible excessive and uncontrolled release of silver ions as well as the release of potentially toxic silver nanoparticles and to improve the mechanical and chemical resistance of the coatings.³ It should be highlighted, however, that Ag ion release was not detected in the present study, remaining thus an important task for future investigations, especially in its dependence on Ag-silica coating thickness.

3.2.1. Microstructural and Compositional Analysis.
3.2.1.1. Sputtering Condition 1 (PEEK/BG/Ag1). Figure 2A,B

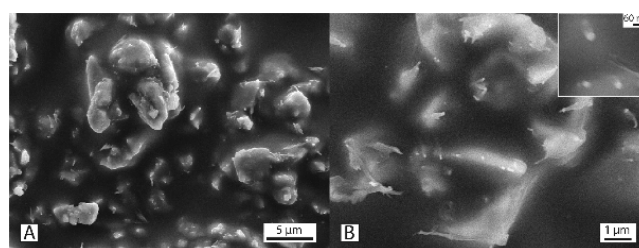


Figure 2. SEM micrographs of RF co-sputtering of silver nanocluster-silica composite obtained by RF co-sputtering on PEEK/BG layer for 15 min (PEEK/BG/Ag1), when 200 W RF and 1 W dc were applied to silica and silver targets, respectively: (A) at low magnification and (B and inset) at higher magnifications.

shows the morphology of the antibacterial coatings sputtered for 15 min on a PEEK/BG layer (PEEK/BG/Ag1). Figure 2A shows the morphological features of PEEK/BG layer (bottom layer), which remain despite the RF sputtering because the coating thickness of the silver nanocluster-silica film (60 nm) is less than the average roughness of the PEEK/BG layer (2.2 ± 0.2). The thickness of the silver nanocluster-silica composite coatings was measured by means of contact surface profiler on

model samples in order to correlate the deposition parameters with the final coating thickness. This procedure confirmed that the coating thickness is homogeneous and reproducible on different substrates. The cross section of the coatings was observed on model samples,³ but not on the ones described in the present paper. Indeed, it was not possible to measure the thickness of the top layer in the present work, because the top layer did not show a clear interface with the PEEK/BG layer due to the high roughness of the electrophoretically deposited PEEK/BG layer. As expected, silver nanoclusters were not visible in SEM images, unless a higher magnification (inset in Figure 2B) was used. Moreover, XPS analysis (Table 1) as well

Table 1. XPS Analysis of the PEEK/BG Layer Coated via RF Co-Sputtering with Silver Nanocluster-Silica Composite for 15 min (PEEK/BG/Ag1) and 40 min (PEEK/BG/Ag2)

element	PEEK/BG	PEEK/BG/Ag1	PEEK/BG/Ag2
C	81.0	31.0	27.8
O	16.9	45.5	47.0
Na	0.9	6.0	7.5
Si		16.4	16.9
S		1.1	0.9
Ag		<0.1	0.1

as EDX analysis (data not shown here) led to the result that the silver amount was below their detection limit. It has been described in the literature that sputtering times of 15 min yield a Ag/(Ag + Si) atomic ratio of 0.37 ± 0.015 .²⁵ However, in the present study it was not possible to measure the actual composition of the top layer due to the complex multilayer structure and high roughness of the underlying PEEK/BG layer. Furthermore, XPS analysis is known to provide surface details; however, due to the high roughness of the PEEK/BG layer the silver nanocluster-silica composite coatings were also deposited in the deeper valleys of the PEEK/BG layers, which could not be detected by XPS.

3.2.1.2. Sputtering Condition 2 (PEEK/BG/Ag2). RF co-sputtering of silver-silica nanocomposite on a PEEK/BG layer for 40 min (PEEK/BG/Ag2) showed a change in color of the obtained coatings. The typical brown color of the coatings was due to the localized surface plasmon resonance (L-SPR) of silver nanoclusters embedded in an amorphous silica matrix.^{2,25} SEM analysis revealed the typical cauliflower-like silica

morphology at high magnification images, as shown in Figure 3B.

XPS analysis showed the relative increase in the amount of silicon and the decrease in carbon content on the surface of coatings (after RF co-sputtering), which confirms the deposition of silver nanoclusters and silica composite on the PEEK/BG layer. Furthermore, an increase in sputtering time (15 to 40 min) did not lead to a significant increase in silver content, as shown by XPS measurements (Table 1, the amount of silver in the two coatings is almost the same). This observation is in accordance with the fact that the only difference between the two coatings is in their thickness.^{12,21,22} Since XPS is a surface sensitive technique, and the penetration depth is around 4–5 nm, XPS is not able to detect differences among the investigated samples in terms of Ag content. However, the available literature reveals that the composition of the top layer under similar sputtering conditions will have a Ag/(Ag + Si) atomic ratio of 0.420 ± 0.002 .²⁵ The RF sputtering process is independent of the substrate material; therefore, we can estimate the composition of the silver nanocluster-silica composite films from the literature.

EDX spectra show the silver peak at the bright spots (Figure 3C), whereas the silver peak was not observed when the spectrum was taken in the silica matrix. The typical nanoporous structure of the coatings was visible at a relatively high magnification, as shown in Figure 3B.

3.2.2. Adhesion Strength. The adhesion strength of the PEEK/BG/Ag layers was analyzed by using the scratch test, as shown in Figure 4. The measured values of Lc1 were very similar for both coatings (PEEK/BG/Ag1, PEEK/BG/Ag2), varying from 3.85 to 4.09 N. At increasing loads (around 10 N), circular cracks appeared on the surface of the PEEK/BG/Ag1 coating, but the coating was still present. The measured values for the second critical load varied from 17.60 to 12.82 N indicating the higher adhesion of the PEEK/BG/Ag1 coating. Yet, it could not be concluded that the silver-silica layer is delaminated from the PEEK/BG layer first or if it is the PEEK/BG coating, which starts to delaminate first because the scratch test (diamond indenter with 1–50 N load) does not allow coating interfaces in the nanometric range to be discerned.

Similarly, FESEM-EDX observations after the scratch test were unable to discern between the two layers of the coating because of the small amount of silver present, which was difficult to detect by EDX. However, the combination of the two coatings, which represents the final coating to be applied

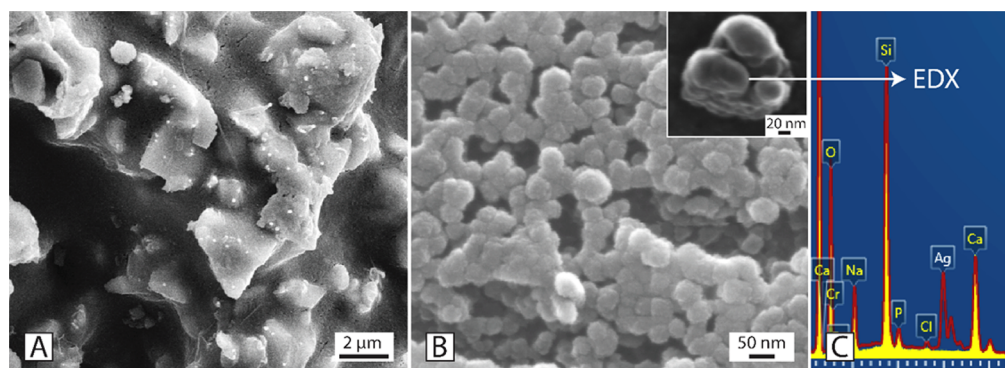


Figure 3. RF co-sputtering of silver-silica nanocomposite on PEEK/BG layer for 40 min (PEEK/BG/Ag2) when 200 W RF and 1 W dc were applied to the silica and silver targets, respectively: (A) SEM micrograph showing the morphology of coatings, (B) high magnification SEM micrograph, and (C) EDX spectrum for the coatings. The red line corresponds to silver particles and the yellow line to the sputtered silica layer.

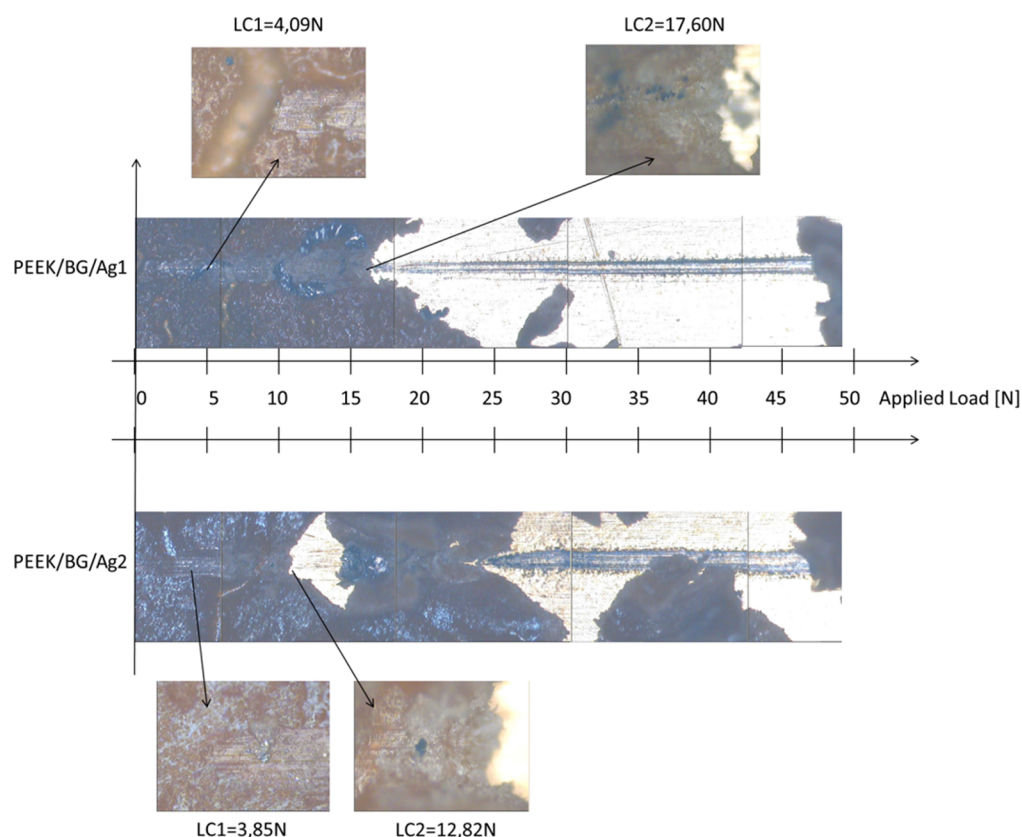


Figure 4. Results of the scratch test for PEEK/BG/Ag1 and PEEK/BG/Ag2 coatings.

and which must sustain the implantation procedure, e.g., friction loads, delaminated if the applied load exceeded 12 N for PEEK/BG/Ag2 and 17 N for PEEK/BG/Ag1, as shown in Figure 4. The adhesion strength measured on the present composite coatings can be considered adequate for their potential orthopedic applications.^{38,39}

3.2.3. Zeta Potential. The zeta potential of the PEEK/BG layer before and after RF co-sputtering of a silver-silica nanocomposite was analyzed by the SurPASS electrokinetic analyzer. The isoelectric point (IEP) of PEEK/BG was about 4, which was hypothesized to be the combination of the high IEP of PEEK (at about 12, as reported for the same PEEK powder used in the present research³¹) and acidic IEP of BG.^{40,41} The IEP of the sputtered coatings was more acidic and close to silica (~3), which confirms a chemical change in the outermost layer of the samples (Figure 5). The difference in the IEP of PEEK/BG/Ag1 and PEEK/BG/Ag2 can be considered negligible, and the two-isoelectric points correlate with the chemical composition of the two layers. Moreover, the authors found the IEP of metallic silver also close to 2. All coatings showed acidic isoelectric points, and consequently, the surfaces would be negatively charged at physiological pH. A plateau in the basic region can be observed in all zeta potential versus pH curves, which can be attributed to the presence of homogeneous functional groups with acidic behavior (e.g., OH groups).^{40,41}

3.2.4. In Vitro Bioactivity Assessment. PEEK/BG/Ag1 and PEEK/BG/Ag2 coatings formed hydroxyapatite after 1 day of immersion in SBF, as shown by SEM, EDX, XRD, and FTIR analyses. Figure 6 shows that platelike apatite crystals completely covered the surface of coatings after 3 days of immersion in SBF. SEM micrographs show the change in

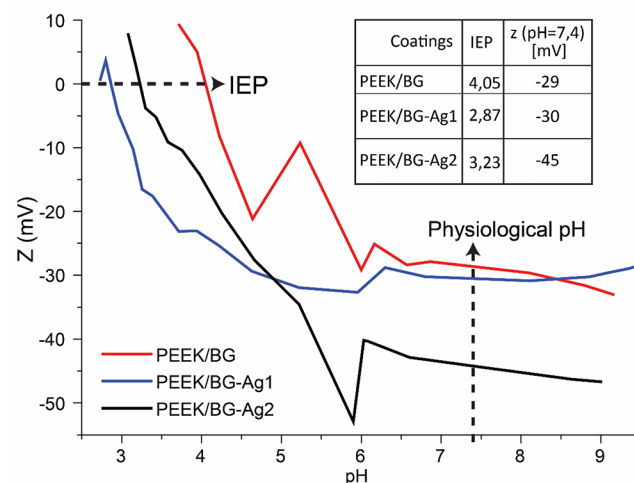


Figure 5. Zeta potential as a function of pH showing IEP, and variations of zeta potential as a function of pH for the PEEK/BG, PEEK/BG/Ag1, and PEEK/BG/Ag2 coatings.

morphology of the coatings after treatment in SBF, such as formation of pores and a nanostructured layer on the coatings (Figure 6). The EDX spectrum demonstrated an increase in the intensity of Ca and P peaks and a decrease in the intensity of Si peaks (Si–O–Si bonds are related to bioactive glass) compared with the coatings before immersion in SBF. The concentration ratio of Ca/P determined from EDX analysis was 1.50, which is below the stoichiometric Ca/P ratio. This may be due to the substitution of Mg in the calcium phosphate structure, as shown in the EDX spectra (Figure 6). Calcium and phosphate ions released from bioactive glass at critical concentration are

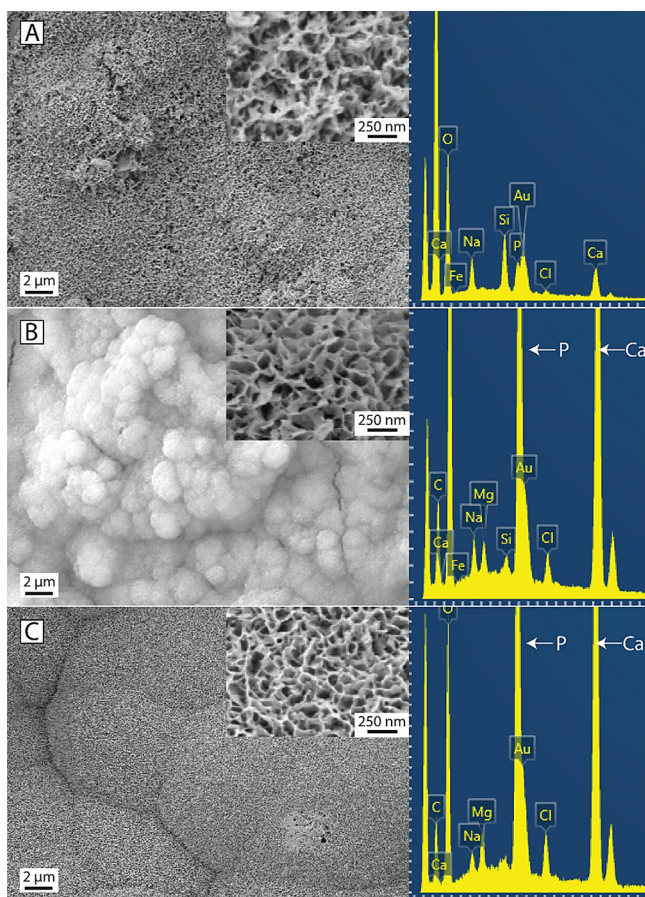


Figure 6. SEM images and EDX analysis of the PEEK/BG/Ag2 coating after immersion in SBF for (A) 1 day, (B) 3 days, and (C) 14 days.

usually considered to lead to the formation of hydroxyapatite on composite coatings.³⁴ Furthermore, FTIR spectra (Figure 7A) show the formation of a new phase after 1 day of

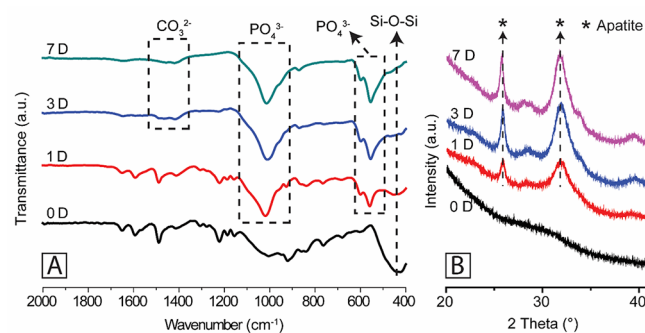


Figure 7. (A) FTIR spectra of a PEEK/BG/Ag2 coating before and after immersion in SBF for 1, 3, and 7 days, and (B) XRD pattern before and after immersion in SBF for 1, 3, and 7 days.

immersion in SBF, for example, reduction in the heights of peaks related to Si–O–Si bonding at 459 cm^{-1} ⁴² and formation of new phosphate (564 , 605 , 963 , 1014 cm^{-1})^{42–45} and carbonate (875 cm^{-1})^{42,44} bonds within 1 day of SBF immersion.⁴⁶ The vibration at 1646 cm^{-1} is due to the adsorbed water in the structure.^{1,9} Moreover, the Si–O–Si peak completely vanished after 14 days of immersion in SBF,

and peaks corresponding to phosphate groups became more intense.

XRD patterns show peaks at $2\theta = 26^\circ$ and 32° , which is the indication of the formation of an apatite-like structure after immersion in SBF (indexed using the Joint Committee on Powder Diffraction Standards card 09-0432),^{1,9,47,48} as shown in Figure 7. Further, the XRD analysis showed an increase in the intensity of the peaks corresponding to apatite with an increase in immersion time in SBF, which indicates a bioactive behavior of coatings (qualitatively).^{1,9,48}

The pH of SBF is 7.40, which is above the IEP of the sputtered and unsputtered coatings. This means that surface charge on the coatings was negative when immersed in SBF, which may lead to the greater absorption of Ca^{2+} ions from SBF solution and may eventually form a crystalline layer of calcium enriched apatite, as shown in SEM images in Figure 6.

On the basis of the above-mentioned results, we conclude that silver nanocluster-silica composite coatings did not affect the initial bioactivity of PEEK/BG layers (as shown in Figure 8). Retention of bioactivity is based on the presence of porosity

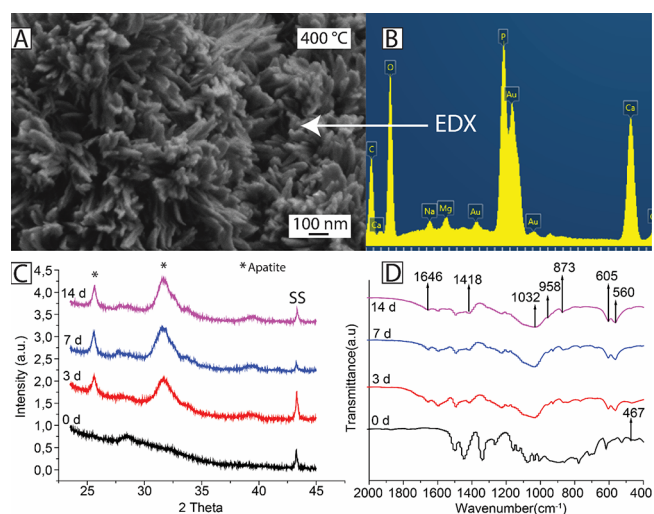


Figure 8. PEEK/BG coatings sintered at $400\text{ }^\circ\text{C}$: (A) SEM image after treatment in SBF for 7 days; (B) EDX analysis after treatment in SBF for 7 days; (C) XRD patterns before and after treatment in SBF for 3, 7, and 14 days; and (D) FTIR spectrum before and after treatment in SBF for 3, 7, and 14 days.

in the composite coatings, which enables bioactive glass particles to come in contact with SBF to form apatite-like crystals. It should also be mentioned that the presence of silica in the RF co-sputtered coatings is not expected to contribute to the bioactive behavior of the coatings, which is dominated by the presence of the highly reactive BG particles.

3.2.5. Antibacterial Studies. The antibacterial activity of PEEK/BG/Ag 1 and PEEK/BG/Ag2 was determined by the formation of an inhibition zone on agar medium by a direct contact method with *E. coli* and *S. carnosus* (Figure 9). The sputtered samples were placed on bacteria-inoculated agar plates. PEEK/BG layers were used as control samples (Figure 9). The control samples of the PEEK/BG layer did not show antibacterial activity. However, PEEK/BG/Ag1 and PEEK/BG/Ag2 developed zones of inhibition against both *E. coli* and *S. carnosus*. The zones of the inhibition halo were measured using “ImageJ” analysis, as illustrated in Table 2.

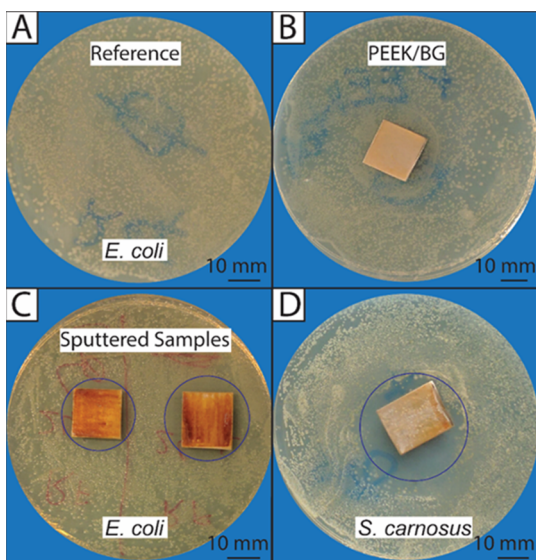


Figure 9. Inhibition halo tests with *E. coli* for (A) reference sample, (B) PEEK/BG (control sample), (C) PEEK/BG/Ag₂, and (D) with *S. carnosus* for PEEK/BG/Ag₂.

Table 2. Antibacterial Disc Susceptibility Tests Showing Relative Diameters of Inhibition after RF Co-Sputtering of Silver-Silica Nanocomposite Coatings on the PEEK/BG Layer^a

material	zone of inhibition halo (mm) against	
	<i>E. coli</i>	<i>S. carnosus</i>
PEEK/BG	0 mm	0 mm
24–1–15 PEEK/BG/Ag ₁	2.5 ± 0.5 mm	5.5 ± 0.5 mm
24–1–40 PEEK/BG/Ag ₂	5.5 ± 0.5 mm	10 ± 1 mm

^aThe PEEK/BG control samples did not develop any inhibition halo zones.

The values in Table 2 indicate that with the increase in sputtering time, the zones of inhibition halo have grown, which is the qualitative indication of the relative increase in antibacterial effect with increasing coating thickness and consequently total silver content. Similar effects have been reported in the literature in that the antibacterial property of silver nanocluster-silica composite coatings increased with an increase in Ag/Si ratio.³ It must be highlighted that very low silver content such as that of PEEK/BG/Ag₁ is sufficient to confer antibacterial activity.

It is worth mentioning that the multistructured PEEK/BG/Ag₁ and PEEK/BG/Ag₂ coatings will enable controlled release of silver ions because the silver nanoparticles are embedded within the silica matrix (the top layer has very fine nanoscale roughness).^{3,22} Thus, the controlled release of silver ions through the silica matrix will minimize possible cytotoxic effects.⁴⁹ Moreover, the deep pores in the PEEK/BG layer may hold the silver nanocluster-silica composite coatings for longer time periods (due to the delayed contact of the coating with the physiological environment). Therefore, the high surface roughness and porosity of the underlying PEEK/BG layer are expected to contribute to the sustained release of silver ions, which will be beneficial for long-term antibacterial effects, and may prevent the potential cytotoxic effect of silver due to possible uncontrolled and rapid release. Furthermore, it has been reported that 0.21 wt % of silver in the coatings may lead

to a cytotoxic effect.⁴⁹ In the present coatings, the concentration of silver ($\leq 0.1\%$) was well below such a cytotoxicity limit.

The formation of an inhibition halo on sputtered samples qualitatively indicates the antibacterial activity of the coatings. The bactericidal property of the silver nanoclusters is associated with the conversion of metallic silver to ionic silver (Ag^+), when exposed to physiological environments. The silver ions are highly reactive toward the electron donor species, such as respiratory enzymes or nucleic acids of bacteria, which can cause the death of bacteria.^{15,19,50} Another mechanism could be the enhanced binding ability of silver ions with the DNA and proteins of bacteria, leading to the penetration of silver ions inside the bacteria and disruption of its DNA replication activity.^{1,4} This metabolic activity of silver nanoclusters causes protein leakage by increasing membrane permeability in bacteria.⁵¹

4. CONCLUSIONS

The conclusions of this article are listed as follows:

- (1) PEEK/BG composite coatings deposited on stainless steel by EPD provided an effective substrate for the deposition of silver nanocluster-silica composite coatings by RF co-sputtering.
- (2) Coatings sputtered at two deposition times showed good adhesion, and complete delamination of the coatings occurs only after the application of a 12–18 N load by the scratch test.
- (3) Sputtered coatings showed the zeta potential to be in the range -35 to -50 mV at physiological pH, which indicates the stability of coatings under physiological conditions.
- (4) Coatings produced by RF co-sputtering did not affect the initial in vitro bioactivity of the PEEK/BG layer.
- (5) Coatings produced by RF co-sputtering of silver nanocluster-silica deposited under both conditions (PEEK/BG/Ag₁, PEEK/BG/Ag₂) confer antibacterial activity against *E. coli* and *S. carnosus*.

This research provides an impetus to PEEK based bioactive coatings to be considered for in vivo investigations and eventually in clinical applications in the orthopedic field. Future work will focus on investigating cell cultures by tracking potential cytotoxic effects due to the release of silver ions. However, the presence of a silica matrix is expected to provide a controlled release of silver ions, which may avoid cytotoxic effects. Antibacterial tests for longer exposure times (>1 day) should be also carried out and correlated with the actual concentration of Ag released.

■ AUTHOR INFORMATION

Corresponding Author

*E-mail: aldo.boccaccini@ww.uni-erlangen.de.

ORCID

Muhammad Atiq Ur Rehman: 0000-0001-5201-973X

Aldo R. Boccaccini: 0000-0002-7377-2955

Author Contributions

M.A.U.R. conducted most of the experimental work and wrote the initial draft of the manuscript. S.F. supported the experimental work and helped in analyzing the results. W.H.G. provided the facilities for conducting the antibacterial test and analyzed the antibacterial results. S.P. performed the

RF sputtering experiments and helped in analyzing the results. F.E.B. helped with the characterization of the coatings and prepared the graphics for the manuscript. Q.N. supported the experiments, in particular the characterization of the coatings. G.G.d.C. performed the scratch test and analyzed the results. M.F. and A.R.B. supervised the whole activity and provided the main idea for this research work. They discussed the results and contributed to the writing of the manuscript. Moreover, all the authors reviewed and provided feedback on the manuscript.

Notes

The authors declare no competing financial interest.

ACKNOWLEDGMENTS

M.A.U.R. wishes to thank the Institute of Space Technology Islamabad, Pakistan, for granting a scholarship and the German Science Foundation (DFG, Go598). The authors would like to thank Barbara Myszkla for XRD analysis and Seray Kaya (both of the Institute of Biomaterials, Department of Material Science and Engineering, University of Erlangen-Nuremberg) for helping in the antibacterial test.

REFERENCES

- (1) Pishbin, F.; Mouriño, V.; Gilchrist, J. B.; McComb, D. W.; Kreppel, S.; Salih, V.; Ryan, M. P.; Boccaccini, A. R. Single-Step Electrochemical Deposition of Antimicrobial Orthopaedic Coatings Based on a Bioactive Glass/chitosan/nano-Silver Composite System. *Acta Biomater.* **2013**, *9*, 7469–7479.
- (2) Ferraris, M.; Balagna, C.; Perero, S.; Miola, M.; Ferraris, S.; Bairo, F.; Battiato, A.; Manfredotti, C.; Vittone, E.; Verne, E. Silver Nanocluster/silica Composite Coatings Obtained by Sputtering for Antibacterial Applications. *IOP Conf. Ser.: Mater. Sci. Eng.* **2012**, *40*, 0–6.
- (3) Ferraris, M.; Perero, S.; Miola, M.; Ferraris, S.; Gautier, G.; Maina, G.; Fucale, G.; Verne, E. Chemical, Mechanical, and Antibacterial Properties of Silver Nanocluster-Silica Composite Coatings Obtained by Sputtering. *Adv. Eng. Mater.* **2010**, *12*, B276–B282.
- (4) Seuss, S.; Heinloth, M.; Boccaccini, A. R. Development of Bioactive Composite Coatings Based on Combination of PEEK, Bioactive Glass and Ag Nanoparticles with Antibacterial Properties. *Surf. Coat. Technol.* **2016**, *301*, 100–105.
- (5) Boccaccini, A. R.; Keim, S.; Ma, R.; Li, Y.; Zhitomirsky, I. Electrophoretic Deposition of Biomaterials. *J. R. Soc., Interface* **2010**, *7*, S581–S613.
- (6) Bairo, F.; Ferraris, S.; Miola, M.; Perero, S.; Verne, E.; Coggiola, A.; Dolcino, D.; Ferraris, M. Novel Antibacterial Ocular Prostheses: Proof of Concept and Physico-Chemical Characterization. *Mater. Sci. Eng., C* **2016**, *60*, 467–474.
- (7) Ouyang, L.; Zhao, Y.; Jin, G.; Lu, T.; Li, J.; Qiao, Y.; Ning, C.; Zhang, X.; Chu, P. K.; Liu, X. Influence of Sulfur Content on Bone Formation and Antibacterial Ability of Sulfonated PEEK. *Biomaterials* **2016**, *83*, 115–126.
- (8) Chen, Q.; Cabanas-Polo, S.; Goudouri, O. M.; Boccaccini, A. R. Electrophoretic Co-Deposition of Polyvinyl Alcohol (PVA) Reinforced Alginate-Bioglass® Composite Coating on Stainless Steel: Mechanical Properties and in-Vitro Bioactivity Assessment. *Mater. Sci. Eng., C* **2014**, *40*, 55–64.
- (9) Pishbin, F.; Mouriño, V.; Flor, S.; Kreppel, S.; Salih, V.; Ryan, M. P.; Boccaccini, A. R. Electrophoretic Deposition of Gentamicin-Loaded Bioactive Glass/chitosan Composite Coatings for Orthopaedic Implants. *ACS Appl. Mater. Interfaces* **2014**, *6*, 8796–8806.
- (10) Zhang, B. G. X.; Myers, D. E.; Wallace, G. G.; Brandt, M.; Choong, P. F. M. Bioactive Coatings for Orthopaedic Implants-Recent Trends in Development of Implant Coatings. *Int. J. Mol. Sci.* **2014**, *15*, 11878–11921.
- (11) Baştan, F. E.; Özbek, Y. Y. Producing Antibacterial Silver-Doped Hydroxyapatite Powders with Chemical Precipitation and Reshaping in a Spray Dryer. *Mater. Tehnol.* **2013**, *47*, 431–434.
- (12) Sathyanarayana, S.; Hübner, C. *Structural Nanocomposites Perspectives for Future Applications*; Njuguna, J., Eds.; Springer: Berlin, 2013.
- (13) Fritsche, A.; Haenle, M.; Zietz, C.; Mittelmeier, W.; Neumann, H. G.; Heidenau, F.; Finke, B.; Bader, R. Mechanical Characterization of Anti-Infectious, Anti-Allergic, and Bioactive Coatings on Orthopedic Implant Surfaces. *J. Mater. Sci.* **2009**, *44*, 5544–5551.
- (14) Nandi, S. K.; Kundu, B.; Datta, S. In *Biomaterials Applications for Nanomedicine*; Pignatello, R., Eds.; InTech, 2011; Chapter 4, pp 69–116.
- (15) Kim, J. S.; Kuk, E.; Yu, K. N.; Kim, J.-H.; Park, S. J.; Lee, H. J.; Kim, S. H.; Park, Y. K.; Park, Y. H.; Hwang, C.-Y.; Kim, Y.-K.; Lee, Y.-S.; Jeong, D. H.; Cho, M.-H. Antimicrobial Effects of Silver Nanoparticles. *Nanomedicine* **2007**, *3*, 95–101.
- (16) Ferraris, M.; Perero, S.; Ferraris, S.; Miola, M.; Vernè, E.; Skoglund, S.; Blomberg, E.; Odnevall Wallinder, I. Antibacterial Silver Nanocluster/silica Composite Coatings on Stainless Steel. *Appl. Surf. Sci.* **2017**, *396*, 1546–1555.
- (17) Maráková, N.; Humpolíček, P.; Kašpárková, V.; Capáková, Z.; Martinková, L.; Bober, P.; Trchová, M.; Stejskal, J. Antimicrobial Activity and Cytotoxicity of Cotton Fabric Coated with Conducting Polymers, Polyaniline or Polypyrrole, and with Deposited Silver Nanoparticles. *Appl. Surf. Sci.* **2017**, *396*, 169–176.
- (18) Mokhena, T. C.; Luyt, A. S. Electrospun Alginate Nanofibres Impregnated with Silver Nanoparticles: Preparation, Morphology and Antibacterial Properties. *Carbohydr. Polym.* **2017**, *165*, 304–312.
- (19) Kim, T.-S.; Cha, J.-R.; Gong, M.-S. Investigation of the Antimicrobial and Wound Healing Properties of Silver Nanoparticle-Loaded Cotton Prepared Using Silver Carbamate. *Text. Res. J.* **2017**, *004051751668863*.
- (20) Wijnhoven, S. W. P.; Peijnenburg, W. J. G. M.; Herberths, C. A.; Hagens, W. I.; Oomen, A. G.; Heugens, E. H. W.; Roszek, B.; Bisschops, J.; Gosens, I.; Van De Meent, D.; Dekkers, S.; De Jong, W. H.; van Zijverden, M.; Sips, A. J. A. M.; Geertsma, R. E. Nano-Silver: A Review of Available Data and Knowledge Gaps in Human and Environmental Risk Assessment. *Nanotoxicology* **2009**, *3*, 109–138.
- (21) Balagna, C.; Perero, S.; Ferraris, S.; Miola, M.; Fucale, G.; Manfredotti, C.; Battiato, A.; Santella, D.; Vernè, E.; Vittone, E.; Ferraris, M. Antibacterial Coating on Polymer for Space Application. *Mater. Chem. Phys.* **2012**, *135*, 714–722.
- (22) Muzio, G.; Perero, S.; Miola, M.; Oraldi, M.; Ferraris, S.; Verne, E.; Festa, F.; Canuto, R. A.; Festa, V.; Ferraris, M. Biocompatibility versus Peritoneal Mesothelial Cells of Polypropylene Prostheses for Hernia Repair, Coated with a Thin Silica/silver Layer. *J. Biomed. Mater. Res., Part B* **2017**, *105*, 1586–1593.
- (23) Surmenev, R. A. Surface & Coatings Technology A Review of Plasma-Assisted Methods for Calcium Phosphate-Based Coatings Fabrication. *Surf. Coat. Technol.* **2012**, *206*, 2035–2056.
- (24) Rabiei, A.; Sandukas, S. Processing and Evaluation of Bioactive Coatings on Polymeric Implants. *J. Biomed. Mater. Res., Part A* **2013**, *101A*, 2621–2629.
- (25) Irfan, M.; Perero, S.; Miola, M.; Maina, G.; Ferri, A.; Ferraris, M.; Balagna, C. Antimicrobial Functionalization of Cotton Fabric with Silver Nanoclusters/silica Composite Coating via RF Co-Sputtering Technique. *Cellulose* **2017**, *24*, 2331–2345.
- (26) Ferraris, S.; Perero, S.; Verne, E.; Battistella, E.; Rimondini, L.; Ferraris, M. Surface Functionalization of Ag-Nanoclusters-Silica Composite Films for Biosensing. *Mater. Chem. Phys.* **2011**, *130*, 1307–1316.
- (27) Prymak, O.; Loza, K.; Tkachev, M. S.; Shulepov, I. A.; Epple, M.; Surmenev, R. A.; Surmeneva, M. A.; Sharonova, A. A.; Chernousova, S. Incorporation of Silver Nanoparticles into Magnetron-Sputtered Calcium Phosphate Layers on Titanium as an Antibacterial Coating. *Colloids Surf., B* **2017**, *156*, 104–113.
- (28) Besra, L.; Liu, M. A Review on Fundamentals and Applications of Electrophoretic Deposition (EPD). *Prog. Mater. Sci.* **2007**, *52*, 1–61.

- (29) Ferrari, B.; Moreno, R. EPD Kinetics: A Review. *J. Eur. Ceram. Soc.* **2010**, *30*, 1069–1078.
- (30) De Riccardis, M. F. In *Ceramic Coatings—Applications in Engineering*; Shi, F., Eds.; InTech, 2012; Chapter 2, pp 43–68.
- (31) Corni, I.; Neumann, N.; Eifler, D.; Boccaccini, A. R. Polyetheretherketone (PEEK) Coatings on Stainless Steel by Electrophoretic Deposition. *Adv. Eng. Mater.* **2008**, *10*, 559–564.
- (32) Boccaccini, A. R.; Peters, C.; Roether, J. A.; Eifler, D.; Misra, S. K.; Minay, E. J. Electrophoretic Deposition of Polyetheretherketone (PEEK) and PEEK/Bioglass® Coatings on NiTi Shape Memory Alloy Wires. *J. Mater. Sci.* **2006**, *41*, 8152–8159.
- (33) Atiq Ur Rehman, M.; Bastan, F. E.; Haider, B.; Boccaccini, A. R. Electrophoretic Deposition of PEEK/bioactive Glass Composite Coatings for Orthopedic Implants: A Design of Experiment (DoE) Study. *Mater. Des.* **2017**, *130*, 223–230.
- (34) Hench, L. L. Bioceramics. *J. Am. Ceram. Soc.* **1998**, *81*, 1705–1728.
- (35) Miola, M.; Vernè, E.; Piredda, A.; Seuss, S.; Cabanas-Polo, S.; Boccaccini, A. R. Development and Characterization of PEEK/B2O3-Doped 45S5 Bioactive Glass Composite Coatings Obtained by Electrophoretic Deposition. *Key Eng. Mater.* **2015**, *654*, 165–169.
- (36) Moskalewicz, T.; Seuss, S.; Boccaccini, A. R. Microstructure and Properties of Composite polyetheretherketone/Bioglass® Coatings Deposited on Ti–6Al–7Nb Alloy for Medical Applications. *Appl. Surf. Sci.* **2013**, *273*, 62–67.
- (37) Kokubo, T.; Takadama, H. How Useful Is SBF in Predicting in Vivo Bone Bioactivity? *Biomaterials* **2006**, *27*, 2907–2915.
- (38) Ma, R.; Tang, T. Current Strategies to Improve the Bioactivity of PEEK. *Int. J. Mol. Sci.* **2014**, *15*, 5426–5445.
- (39) Moskalewicz, T.; Zych, A.; Lukaszczyk, A.; Cholewa-Kowalska, K.; Kruk, A.; Dubiel, B.; Radziszewska, A.; Berent, K.; Gajewska, M. Electrophoretic Deposition, Microstructure, and Corrosion Resistance of Porous Sol-Gel Glass/Polyetheretherketone Coatings on the Ti-13Nb-13Zr Alloy. *Metall. Mater. Trans. A* **2017**, *48*, 2660–2673.
- (40) Spriano, S.; Sarath Chandra, V.; Cochis, A.; Uberti, F.; Rimondini, L.; Bertone, E.; Vitale, A.; Scolaro, C.; Ferrari, M.; Cirisano, F.; Gautier di Confiengo, G.; Ferraris, S. How Do Wettability, Zeta Potential and Hydroxylation Degree Affect the Biological Response of Biomaterials? *Mater. Sci. Eng., C* **2017**, *74*, 542–555.
- (41) Cazzola, M.; Corazzari, I.; Prenesti, E.; Bertone, E.; Vernè, E.; Ferraris, S. Bioactive Glass Coupling with Natural Polyphenols: Surface Modification, Bioactivity and Anti-Oxidant Ability. *Appl. Surf. Sci.* **2016**, *367*, 237–248.
- (42) Kharaziha, M.; Fathi, M. H. Synthesis and Characterization of Bioactive Forsterite Nanopowder. *Ceram. Int.* **2009**, *35*, 2449–2454.
- (43) Stanciu, G.; Sandulescu, I.; Savu, B. Investigation of the Hydroxyapatite Growth on Bioactive Glass Surface. *J. Biomed. Pharm. Res.* **2007**, *1*, 34–39.
- (44) Liu, X.; Ding, C.; Wang, Z. Apatite Formed on the Surface of Plasma-Sprayed Wollastonite Coating Immersed in Simulated Body Fluid. *Biomaterials* **2001**, *22*, 2007–2012.
- (45) Khalili, V.; Khalil-Allafi, J.; Frenzel, J.; Eggeler, G. Bioactivity and Electrochemical Behavior of Hydroxyapatite-Silicon-Multi Walled Carbon Nano-Tubes Composite Coatings Synthesized by EPD on NiTi Alloys in Simulated Body Fluid. *Mater. Sci. Eng., C* **2017**, *71*, 473–482.
- (46) Heise, S.; Höhlinger, M.; Hernández, Y. T.; Palacio, J. J. P.; Rodriguez Ortiz, J. A.; Wagener, V.; Virtanen, S.; Boccaccini, A. R. Electrophoretic Deposition and Characterization of Chitosan/bioactive Glass Composite Coatings on Mg Alloy Substrates. *Electrochim. Acta* **2017**, *232*, 456–464.
- (47) Shoaib, M.; Saeed, A.; Akhtar, J.; Rahman, M. S. U.; Ullah, A.; Jurkschat, K.; Naseer, M. M. Potassium-Doped Mesoporous Bioactive Glass: Synthesis, Characterization and Evaluation of Biomedical Properties. *Mater. Sci. Eng., C* **2017**, *75*, 836–844.
- (48) Cordero-Arias, L.; Boccaccini, A. R. Electrophoretic Deposition of Chondroitin Sulfate-Chitosan/bioactive Glass Composite Coatings with Multilayer Design. *Surf. Coat. Technol.* **2017**, *315*, 417–425.
- (49) Simchi, A.; Tamjid, E.; Pishbin, F.; Boccaccini, A. R. Recent Progress in Inorganic and Composite Coatings with Bactericidal Capability for Orthopaedic Applications. *Nanomedicine* **2011**, *7*, 22–39.
- (50) Devi, G. K.; Kumar, K. S.; Parthiban, R.; Kalishwaralal, K. An Insight Study on HPTLC Fingerprinting of Mukia Maderaspatna: Mechanism of Bioactive Constituents in Metal Nanoparticle Synthesis and Its Activity against Human Pathogens. *Microb. Pathog.* **2017**, *102*, 120–132.
- (51) Yuan, Y.-G.; Peng, Q.-L.; Gurunathan, S. Effects of Silver Nanoparticles on Multiple Drug-Resistant Strains of Staphylococcus Aureus and Pseudomonas Aeruginosa from Mastitis-Infected Goats: An Alternative Approach for Antimicrobial Therapy. *Int. J. Mol. Sci.* **2017**, *18*, 569.